Structural characterization of the packings of granular regular polygons

Chuncheng Wang,[1] Kejun Dong,[2,*] and Aibing Yu[1]

[1]*Laboratory for Simulation and Modeling of Particulate Systems, Department of Chemical Engineering, Monash University, Clayton, Victoria 3800, Australia*

[2]*Institute for Infrastructure Engineering, Western Sydney University, Penrith NSW 2751, Australia*

(Received 3 September 2015; revised manuscript received 8 November 2015; published 7 December 2015)

By using a recently developed method for discrete modeling of nonspherical particles, we simulate the random packings of granular regular polygons with three to 11 edges under gravity. The effects of shape and friction on the packing structures are investigated by various structural parameters, including packing fraction, the radial distribution function, coordination number, Voronoi tessellation, and bond-orientational order. We find that packing fraction is generally higher for geometrically nonfrustrated regular polygons, and can be increased by the increase of edge number and decrease of friction. The changes of packing fraction are linked with those of the microstructures, such as the variations of the translational and orientational orders and local configurations. In particular, the free areas of Voronoi tessellations (which are related to local packing fractions) can be described by log-normal distributions for all polygons. The quantitative analyses establish a clearer picture for the packings of regular polygons.

DOI: 10.1103/PhysRevE.92.062203 PACS number(s): 81.05.Rm, 61.43.Gt

I. INTRODUCTION

Particle packing is of fundamental importance to granular materials which are commonly encountered in nature and industry [1,2]. It is also of great interest to various topics in physics and mathematics [3,4], including jamming states, self-assembly, glass transition, and optimization problems. However, particle packing is still far from well understood. Essentially, packing structure, which determines the properties of a packing, is still not able to be predicted by a general model that can consider various controlling variables, from material properties to packing methods. Previously, the majority of work has been done for spherical particles. Significant progress has been made in characterizing the structures of the packings of monosize to multisize [5] and noncohesive to cohesive spheres [6] in terms of different structural parameters, such as the radial distribution function, coordination number, bond-orientation order, Voronoi and Delaunay tessellations [7,8], and clusters [9,10]. These analyses have improved the understanding of the packing structures of spheres [11] and facilitated theoretical modeling [12,13].

However, in nature particles are generally not spherical and particle shape plays an important role in controlling packing structures [14]. A number of studies have been conducted for the packings of particles of different shapes, e.g., ellipses [15,16] and polygons [17–19] in two dimensions (2D) and polyhedral [20,21], ellipsoids [14,22], and cylinders [23,24] in three dimensions (3D), etc. In particular, great efforts have been made in the pursuit of the densest packings, some of which have even overturned our previous understanding [14,20]. On the other hand, for the random packings of nonspheres, mean-field theory has been attempted [23]. These studies have gradually revealed the controversial effect of particle shape on particle packing. However, compared to the enormous research on the structures of sphere packings, the structures of nonsphere packings are very poorly understood.

Theoretically particle packing can be in any dimensions. Granular packings are generally in 3D. However, the packings of nonspherical particles in 2D have also attracted increasing interest in recent years. Such packings are related to not only the applications of certain low-dimensional particles, such as films and monolayers, but also the self-assembly and phase transition of 2D colloidal systems [25,26]. Two kinds of shapes are typical for the 2D nonspherical particles, namely, polygons and ellipses. For polygons, it is found that regular triangle, square, and hexagon have higher packing fractions than others as they can perfectly fill a two-dimensional space [19]. However, other regular polygons also present rich crystalline and/or quasicrystalline packing structures [17,27].The effects of packing method and size distribution on these packings have also been studied recently [28,29]. For ellipses, the highest packing fraction can be found at an aspect ratio of 1.6 [15], and clusters of ellipses with similar orientations can be clearly identified when the aspect ratio is high, with large-size voids between clusters [16].

In these studies, however, the packing structures have not been comprehensively characterized. For example, the structural analyses are often limited to coordination number, with only a few radial distribution functions given. In particular, the Voronoi tessellation analysis, which is very useful in linking the local and global packing properties [23], is rather limited. This may be due to the difficulty in obtaining the Voronoi tessellations for the packings of nonspherical particles, although some efforts have been made [30,31]. On the other hand, structural analyses related to phase transitions have been performed on the jamming or annealing of the thermal nonspherical particle systems [25,32,33], but these systems may not be exactly the same as the mechanical stable packings of granular particles under gravity, in which the mechanical contact forces such as friction play more important roles, though some results can be comparable to the granular packings, similar to the comparative studies between the critical states of granular sphere packings and the phase transitions of hard sphere systems [9,11].

*Kejun.Dong@westernsydney.edu.au

In this work, we investigate the effects of edge numbers (n) and sliding friction coefficient (μ) on the packings of regular polygons. The packings are simulated by using the discrete element method (DEM). Compared to experiments, DEM simulation provides a more easily controlled and cost-effective way to obtain packing structures. Unlike other simulation methods, such as the random absorption and global rearrangement methods, DEM uses first principles to model the motion of each particle without any arbitrary assumptions and considers the forces between particles in a more realistic way. It has been testified that DEM can generate more comparable results to experimental data for the packings of granular beads [34,35]. By using DEM, the packings of regular polygons are obtained and the structures are characterized in terms of the radial distribution function, coordination number, and Voronoi tessellation. The results quantify different structural features for the packings of granular regular polygons, which can not only improve the understanding on the effects of shape and friction on these packings, but also pave a way to the theoretical modeling of the packing structures of nonspherical particles.

II. METHOD DESCRIPTION

A. Simulation method and conditions

A recently developed method called ODDS (orientation discretization database solution) has been adopted in DEM to simulate the packings of nonspherical particles. This method can handle the different types of contacts between two polygons, such as edge-to-edge, vertex-to-vertex. and vertex-to-edge contacts in a uniform scheme. The method has been validated by a wide range of agreements with experimental data. The details of the simulation algorithm can be found in Dong *et al.* [36]. The nonspherical particles studied in this work include regular polygons with three to 11 edges. Table I lists the material properties and other controlling parameters adopted in the simulations. The size of a particle, d, is the diameter of the circumcircle of the polygon. Figure 1 schematically shows the simulation setup and process. Initially, the particles are generated randomly in a container with width of $50d$ (X axis) and height of $300d$ (Y axis). The number of particles is adjusted for different shapes in order to make a consistent initial porosity, $\varepsilon \approx 0.9$. The particles are then settled under gravity along the–Y direction. Periodic boundary conditions are applied along the X axis and a bottom plane is put at $Y = 0$. Note that unlike in previous studies [17–19] where the packings of polygons were obtained from isotropic contraction or compression of random generated particles without gravity, the packing method here is similar to the pour packing in experiments [2,22,24], and it has been widely used in the DEM simulations of granular packings [5–7,15,22,36].

TABLE I. Material properties of the particles and other controlling parameters used in the simulations.

Parameter	Value
Young's modulus, Y	1.0×10^7Pa
Poisson's ratio, σ	0.29
Normal damping coefficient, γ^n	0.3
Normal damping coefficient, γ^t	0.2
Sliding friction coefficient, μ	0.1−0.9
Rolling friction coefficient, μ_r	0.005
Particle size, d	1 mm
Particle density, ρ	2.5×10^3kg/m^3
Time step, Δt	$2 \times 10^{-7}s$
Particle number	3000–10000

In the simulations, the translational and rotational motions of the particles are governed by Newton's second law and the governing equations are solved by time integration. When a particle has an overlap with another particle or a wall, the contact force and torque between them are calculated based on the overlap. The dynamic packing process finishes and a stable structure is obtained when the velocities and rotations of all particles diminish to nearly zero due to the energy dissipations in the particle-particle and particle-wall collisions. The packing fraction is measured in this final state. Different polygons and/or with different sliding frictions may generate different packing fractions through their effects on the particle-particle and particle-wall in8teractions, while there are no other rules in controlling the packing fraction. Although packed under gravity, the simulated packings are homogeneous, which can be seen from Fig. 2. For each packing, ρ measured with different heights just fluctuates slightly but deviates obviously only when the height is too low or too high, which is due to the boundary effect. Similar to the treatments in the previous studies [6,22,36], the particles in the top and bottom regions of $5d$ thick are not included in our analyses to eliminate such effect.

Generally a packing system with given controlling variables, including well-defined packing method, should yield reproducible packing fractions. To validate the reproducibility of our results, we have first tried the simulations with different dimension sizes. Figure 3 demonstrates that when the width of the simulation zone is larger than $20d$, the variations of packing fraction are negligible. Secondly, we have tried particles with different randomized initial positions and orientations. As shown in Fig. 4, the resulting packing fractions are also nearly the same for a kind of regular polygon with a specific sliding fraction coefficient. For all the tested cases, the variations of ρ are within ± 0.005, which confirms the reproducibility of our results.

B. Voronoi tessellation by using space discretization

Although Voronoi tessellation has a simple definition, to obtain such tessellations for a packing of nonspherical particles is not easy in an analytical way. Originally Voronoi tessellation is applied to a set of seed points in a space. For a given seed point, the region consisting of all points closer to it than to any other seed points is defined as its Voronoi tessellation. When it is extended to the assembly of particles, the Voronoi tessellation of a particle contains the points with distance to its surface no greater than those to other particles. For uniform spheres, such a Voronoi tessellation can be obtained by the intersecting of the bisect planes between a particle and its neighbors, which always gives a polyhedron (or polygon in 2D). This method can be extended to radical tessellations for multisized spheres. Several open-source programs have been developed to obtain the Voronoi or radical tessellations for sphere packings; e.g.,

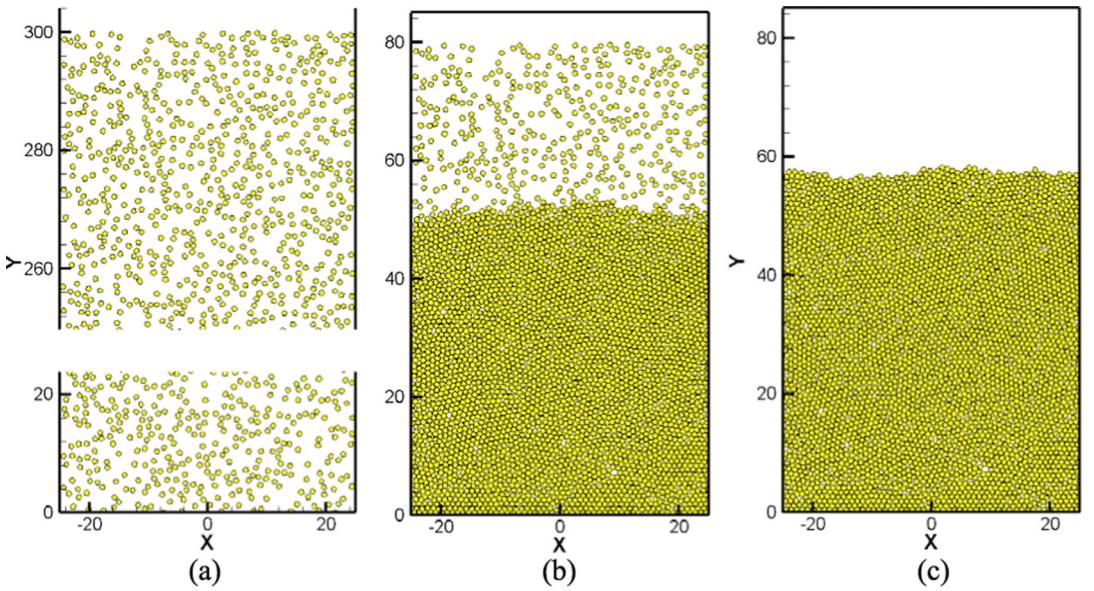

FIG. 1. (Color online) Snapshots show the formation of a packing of regular pentagons at (a) 0 s; (b) 0.11 s; and (c) 0.3 s.

see recent work done by VORO + + [5,37]. For nonspherical particles, however, the Voronoi tessellations could have curved surfaces, and are called Voronoi *S* regions [30,38]. As the distance of a point to a nonspherical particle surface is often much more complicated than that of a spherical particle, there is no simple method to obtain the Voronoi tessellations for general nonspherical particles. Several advanced algorithms have been developed [30,31]. A more simple and universal numerical method has been proposed in x-ray tomography [39], which is used in this work and briefly described below.

After obtaining a packing, we first digitize the whole packing space into an image composed of finite pixels. The pixels inside the particles (with its center inside) are labeled "0" and other pixels "1," as shown in Fig. 5(a). Then the boundary pixels are identified by checking the surrounding pixels. After that, we "burn" those void pixels adjacent with the identified boundary pixels of all particles simultaneously, which yields a layer of pixels with 1 pixel distance from the particle boundary [see Fig. 5(b)]. These "burned" pixels are then treated as the "new" boundary pixels and the last step will be reiterated. The medial axes of the voids are obtained when two or more "fires" meet, which are equidistant to the surface of at least two particles. The obtained medial axis of voids constructs the boundaries of the Voronoi tessellations, and the pixels burned from the boundary of a particle are closer to that particle than to any other ones, which construct the inside space of the Voronoi tessellation. This method is general to any convex shapes and is simple to be realized in a computer program though other methods can also be used for obtaining the Voronoi tessellation for the studied packings [31]. The obtained Voronoi tessellations conform to the genuine definition while the errors can be controlled by using enough fine pixels. Figure 5(c) shows the Voronoi tessellations

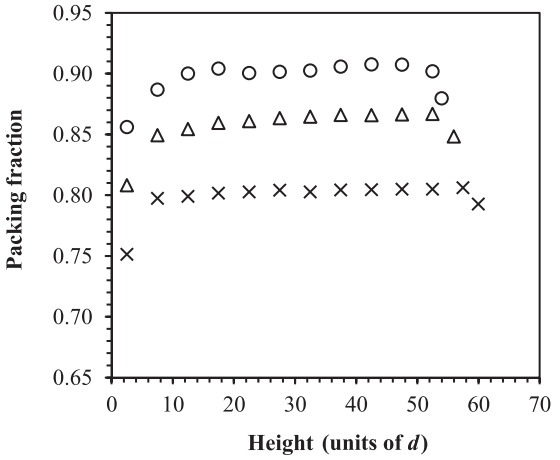

FIG. 2. Packing fraction measured with different heights for the packings of regular polygons with different edge numbers and sliding friction coefficients: ◯, $n = 4$, $\mu = 0.1$; Δ, $n = 9$, $\mu = 0.3$; ×, $n = 5$, $\mu = 0.9$.

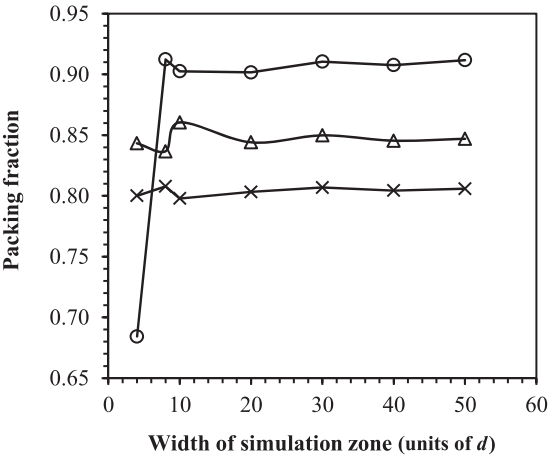

FIG. 3. Packing fraction as a function of the width of the simulation zone for different polygons: ◯, $n = 4$, $\mu = 0.1$; Δ, $n = 9$, $\mu = 0.3$; ×, $n = 5$, $\mu = 0.9$.

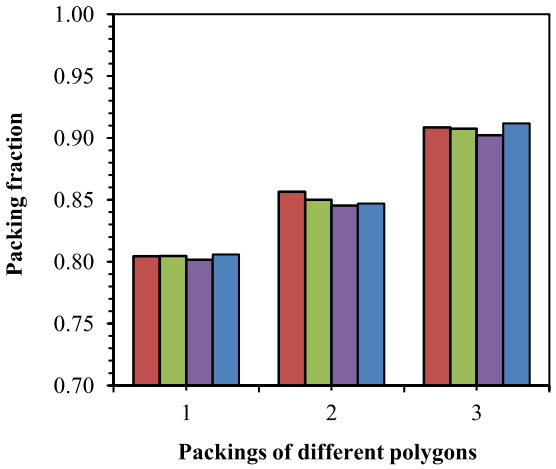

FIG. 4. (Color online) Comparison of packing fractions obtained using particles with different randomized initial positions and orientations. Each bar represents a simulation case: group 1, $n = 5$, $\mu = 0.9$; group 2, $n = 9$; group 3, $n = 4$, $\mu = 0.1$.

for a packing of polygons obtained by the proposed method as an example.

III. RESULTS AND DISCUSSION

A. Packing fraction

We firstly investigate the simulated packings in a global scale. Figure 6 visualizes the final packing structures obtained for different polygons. The particles are colored by their local packing fractions obtained from Voronoi tessellations which will be discussed later. It can be seen that for all regular polygons, there are always some densely packed regions in the packings and the boundaries between them are loosely packed regions with relatively large voids, which are similar to the clusters and voids found in the piling of ellipses [16]. Generally the dense regions become larger with the increase of edge number. However, these regions have different configurations for different polygons, which are mainly dependent on whether the polygon shape is geometrically frustrated or not. It is known that the regular polygons can be classified into two groups: Group 1 (G1) includes regular triangle, square, and hexagon, which are able to fill a plane perfectly, and Group 2 (G2) contains all other regular polygons which cannot. As can be seen from Fig. 6, for G1 polygons, the densely packed regions can be almost with no voids and the local packing fractions reach nearly 1.0, while for G2 polygons, there are still voids in the these regions with the local packing fractions obviously lower than 1.0. For G1 polygons, particles have almost perfect edge-edge contacts in the dense regions, while for G2 polygons, the contacts are more diversified with imperfect edge-edge and also edge-vertex contacts. On the other hand, the densely packed regions for G2 polygons are mostly hexagonal lattice structures which are similar to those of the dense packings of disks, especially when the edge number is large [e.g., $n = 11$, Fig. 6(d)]. This trend has also been observed by Ciesla and Barbasz [28].

Figure 7 shows the packing fraction ρ for the simulated packings. It can be seen that generally G1 polygons possess higher ρ than G2 polygons as they are not geometrically frustrated. In G1, the regular hexagon yields the highest ρ while regular triangle the lowest, which is in agreement with the results obtained by Mirghasemi *et al.* [19]. The regular pentagon, although it has an edge number between those of square and regular hexagon, yields a significantly lower ρ than the other two shapes as it belongs to G2. Note the packing fraction of regular pentagon at $\mu = 0.1$ is 0.850, which is in agreement with the value 0.85 obtained in the contact dynamics simulations of frictionless pentagons [29] and close to the value 0.84 obtained in a Monte Carlo simulation of hard pentagons when phase transition occurs [32]. For G2 polygons, the regular heptagon has the lowest ρ, which is in line with the hypothesis that this shape has the lowest packing fraction for the densest packings of regular polygons

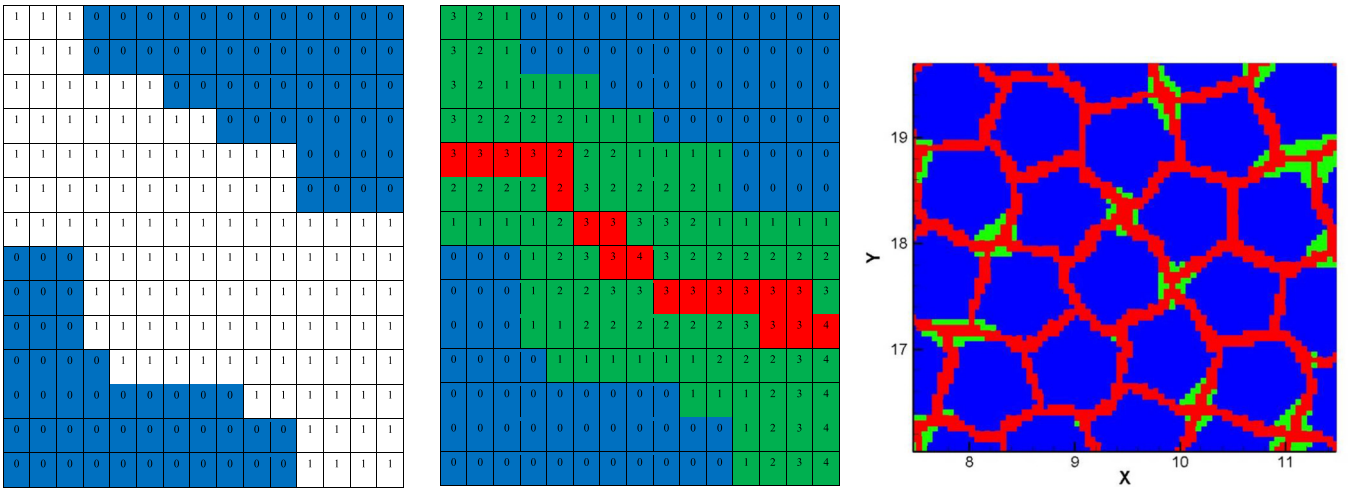

(a) (b) (c)

FIG. 5. (Color online) Digitized Voronoi tessellation. (a) Particle identification. Pixels of particles are labeled "0" and those of voids "1." (b) Distance transformation of voids from the boundary of particles. (c) Obtained Voronoi tessellations for a packing of pentagons. Particles, pores, and boundaries of Voronoi tessellations are colored in blue (dark gray), green (light gray), and red (medium gray), respectively.

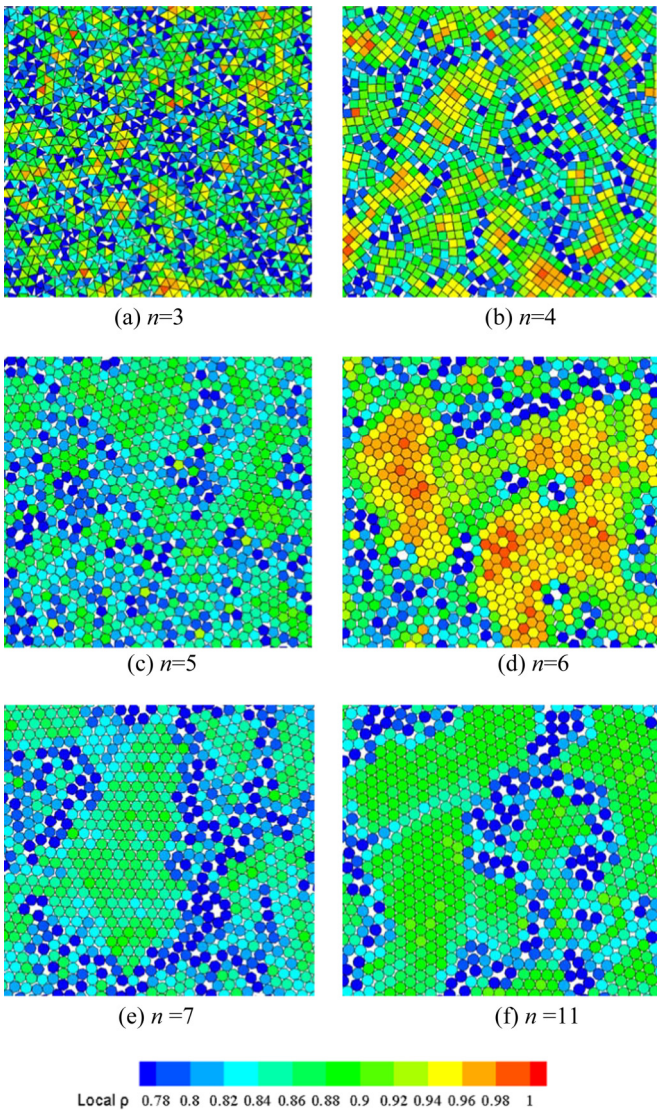

FIG. 6. (Color online) Simulated packings of regular polygons with different edge numbers. Particles are colored according to their local packing fractions.

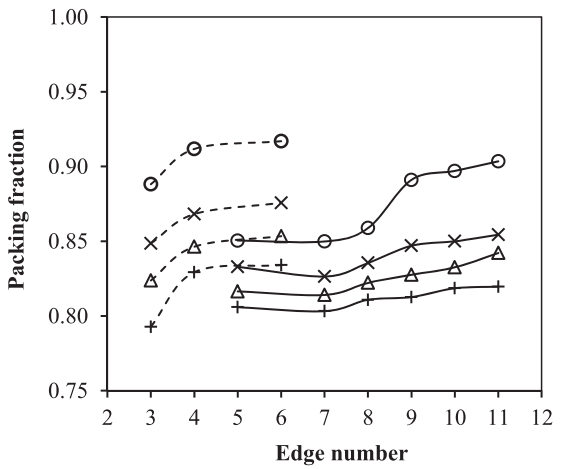

FIG. 7. Packing fraction as a function of polygon edge number under different sliding friction coefficients: ◯, $\mu = 0.1$; ×, $\mu = 0.3$; Δ, $\mu = 0.5$; +, $\mu = 0.9$.

[17]. When the edge number n increases from 7, ρ increases monotonically and approaches that of the densest packing of disks [$\pi/(2\sqrt{3}) \approx 0.907$] at the large n. These changes are in agreement with the observations in other studies [17,28,40], but different from Mirghasemi *et al.* [19] in which ρ decreases with n when $n > 6$. Such a difference probably results from the different packing methods, as in the other study [19] the packings are obtained from isotropic compression, so that the particles may be difficult to rearrange under the constrain of the compressive force. On the other hand, a higher sliding friction coefficient always leads to a lower packing fraction for all kinds of regular polygons. This is in agreement with the effect of friction on the packings of granular spheres and nonspheres in three dimensions [22,36] and will be further discussed.

B. Radial distribution function

Packing fraction is only a global structural parameter, whereas the microstructure of a packing is rather complicated and normally needs to be characterized by different parameters. The radial distribution function (RDF), which quantifies the possibility of finding another particle at a given distance r from the reference particle, is a very useful indicator of the translational order of a packing. The RDF is shown in Fig. 8 for the packings of the regular polygons. The curves generally have the first and highest peak at a minimum r. And with the increase of r, subpeaks emerge at different positions for different polygons but gradually diminish. At a large r, the curves just slightly fluctuate near 1. Such kind of RDF curve indicates that these packings have translational orders to certain ranges, but are still disordered in the long range.

The heights and positions of the RDF peaks represent the specific translational orders of the systems and are normally called characteristic peaks. We look at the positions first. Figure 9(a) shows the radial distances of the first and second RDF peaks for different regular polygons. These values are compared to the distance between two polygons with perfect edge-edge contact, given by $d_e = d\sin(\frac{\pi}{n})$, and the average contacting distance d. Here we consider the two contacting polygons with random orientations as shown in Fig. 9(b), and the average contacting distance d is defined as $\langle d\rangle = \frac{1}{4\pi^2}\int\int_0^{2\pi} r(\theta_1,\theta_1)d\theta_1 d\theta_2$, which is obtained by numerical integration. For G1 polygons, the first and highest peak is always at $r = d_e$. Actually, the positions of the ssubpeaks after the second peak are generally corresponding to the structures perfectly packing the whole space, in which a polygon always has perfect edge-edge contacts with other ones, as demonstrated in the inset figures in Fig. 8. Interestingly, for $n = 3$ and 4, the second peak is at $r = d$, showing a certain ratio of contacting polygon pairs in random orientations. Such a subpeak cannot be found in the RDF of regular hexagon, indicating that packings of regular hexagons are more ordered than those of regular triangles and squares. For G2 polygons, the positions of the first RDF peak are not at $r = d_e$ but rather close to $r = d$, except for regular pentagon. This indicates that for these regular polygons, two contacting polygons are mostly random oriented which does not favor any specific configurations. The regular pentagon is special, as besides a strong peak at $r = d$, there is another

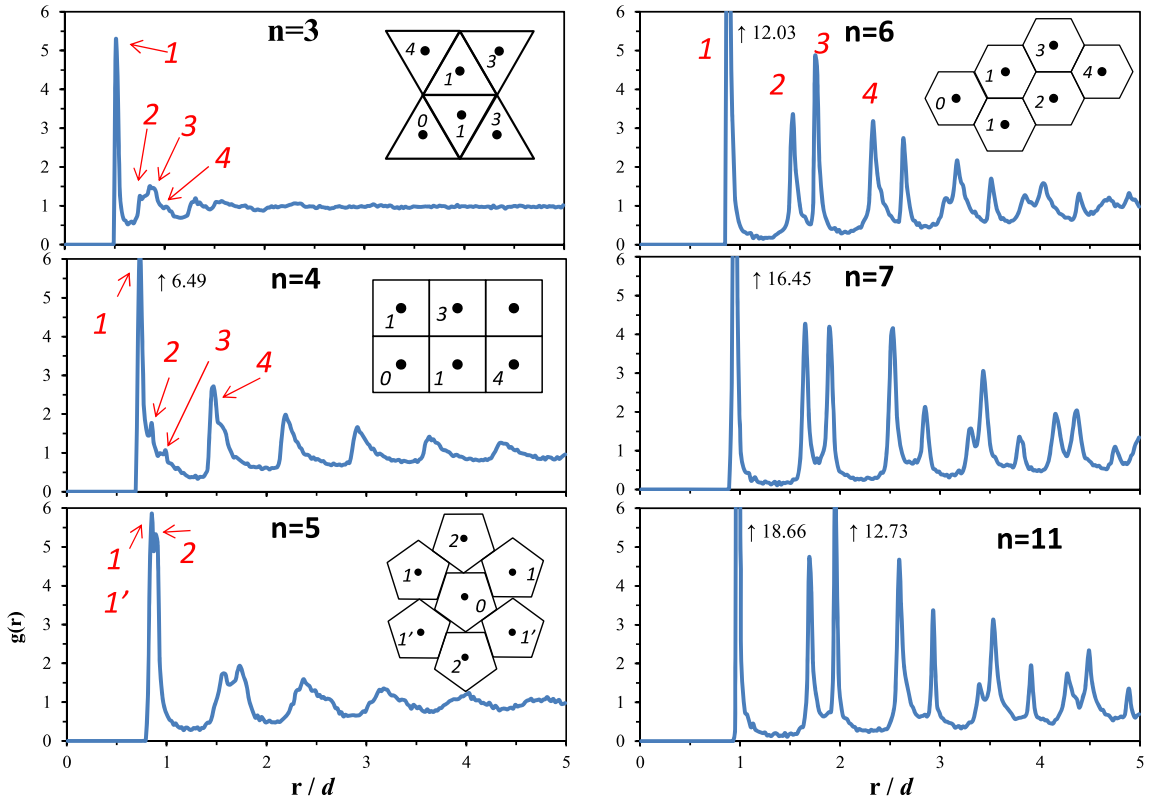

FIG. 8. (Color online) Radial distribution functions of regular polygons with different edges at $\mu = 0.3$. Insets show the neighbor particles that represent the peaks.

strong peak corresponding to a quasicrystalline structure as demonstrated in the inset figure. This structure is shown to be more mechanically stable [17] than other possible quasicrystalline structures of regular pentagons [27], and has also been identified in other pentagon packings [29,32]. Note that the nearest and second nearest neighboring particles in this structure have similar distances ($r = 0.829d$ and $r = 0.861d$, respectively) to the center particle, which thus merge into one peak ($r = 0.845d$). Such a peak has also been observed in the packing of frictionless pentagons [29], but is not evident in the Brownian pentagons even at a high volume fraction 0.88 [25], indicating that the related quasicrystalline structure is very sensitive to the thermal perturbations. With the further increase of r, all the G2 polygons show the subpeaks at about $r = \sqrt{3}d, 2d, \sqrt{7}d, \ldots$, corresponding to the hexagonal lattice structure.

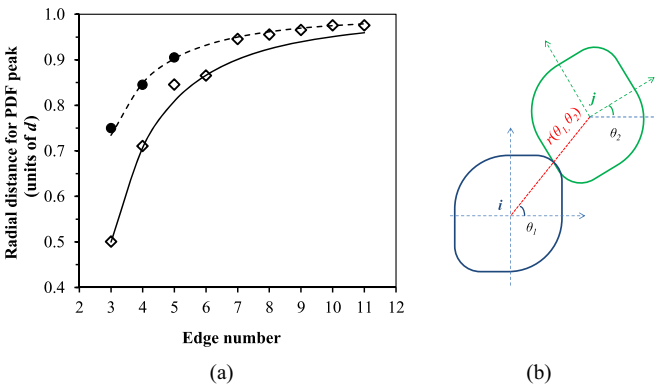

FIG. 9. (Color online) (a) Symbols are the radial distances of the first RDF peak (◇) and second RDF peak (•) versus the edge number for the packings of regular polygons ($\mu = 0.3$). The solid line is the distance between two polygons with perfect edge-edge contact. The dashed line is the averaged distance between two contacting polygons with random orientations. (b) Schematic of two contacting particles.

Secondly, when looking at the heights of the peaks, it can be seen that with the increase of n, the first peak is normally higher and the subpeaks more distinct, demonstrating an increase in the short-range translational order. In particular, for G1 polygons, regular triangle has the lowest peaks, regular hexagon the highest, and square in between. Therefore even all of them can form the maximum densest packing with $\rho = 1$; regular triangle yields the lowest ρ and regular hexagon the highest. This is probably because the particles are randomly oriented at the beginning and need to be rearranged to form a denser structure, in which less rotation is required for a polygon of a higher n than that of a lower n, as the former has a higher order rotational symmetry.

Figure 10 further shows the effect of sliding friction coefficient on the RDF. For all these polygons, the change of μ does not alter the positions but just the heights of the peaks. With a lower μ, the peaks become higher and more distinct, showing that the system's translational order is increased. Accordingly packing fraction increases. This is also different from the colloidal systems composed of polyhedral particles, in which the peaks will emerge or disappear in the

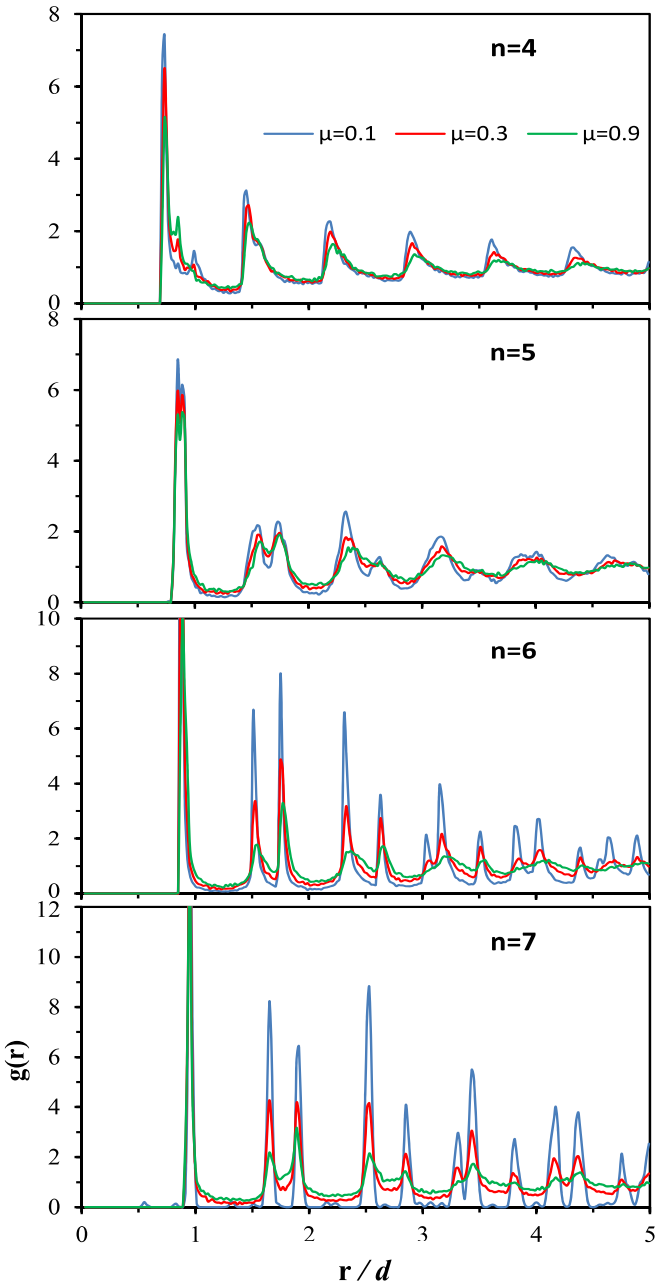

FIG. 10. (Color online) Radial distribution functions of regular polygons with different edges under different sliding friction coefficients: blue, $\mu = 0.1$; red, $\mu = 0.3$; green, $\mu = 0.9$.

RDF when ρ varies [25,26], as a granular packing is always a jammed athermal system and the colloidal particles are affected by the thermal perturbations, which are likely to bring or eliminate specific translational orders. On the other hand, under the athermal condition the effect of friction on the extent of translational order is shown to be important and deserves further study.

C. Coordination number

Another common structural parameter to characterize a packing is the coordination number (CN), which is the number of the contacting particles of a given one. Figure 11 shows the mean coordination number, ⟨CN⟩, for the packings of different polygons under different sliding friction coefficients. Note that to avoid numerical round-off errors, two particles are regarded as in contact when their surface distance is less than a cutoff value $0.02d$, which is similar to the treatment in analyzing sphere packings [11].

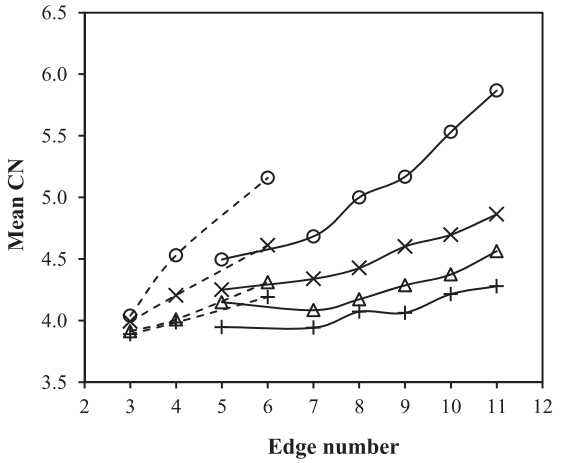

FIG. 11. Mean coordination number of the packings of regular polygons as a function of polygon edge number under different sliding friction coefficients: ◯, $\mu = 0.1$; ×, $\mu = 0.3$; Δ, $\mu = 0.5$; +, $\mu = 0.9$.

From Fig. 11, firstly it can be seen that ⟨CN⟩ is between 3.8 and 5.8, which are close to the theoretical bounds 4 and 6 given by the isostatic conjecture for 2D ellipses [14,15]. However, here the bounds are related to the specific local structures formed by different polygons. The lower bound 3.8 is given by the packing of regular triangles, in which a perfectly ordered structure actually gives CN = 3 with three triangles enclosing a central one. However, with a slight distortion, an extra neighbor triangle may be added, as indicated by the second peak of the RDF (Fig. 8). On the other hand, the upper bound 5.8 is given by regular hendecagon rather than regular hexagon, as regular hendecagon is close to disk in shape and hence easily forms the hexagonal lattice structure.

The relationship between ⟨CN⟩ and n can also be divided into G1 and G2 as shown in Fig. 11. For both groups, ⟨CN⟩ increases with the increase of n and the decrease of μ. And with the increase of n, the effect of μ on ⟨CN⟩ becomes more profound. This is probably also because the rearrangement of a regular polygon with more edges requires less rotation. When $\mu \geqslant 0.3$, ⟨CN⟩ for regular hexagon is always the highest, whereas when μ is decreased to 0.1, ⟨CN⟩ of G2 polygons increases more sharply with n, and ⟨CN⟩ for regular hendecagon is even larger than that of regular hexagon and closer to 6, probably because the hexagonal lattice of regular hendecagon can stand more distortions than that of regular hexagon.

The relationship between CN and ρ is always interesting to researchers as it can be related to the modeling of ρ by isostatic conjecture [13,14]. From the application view, such relationships can help model transport properties of packings using a single macroscopic parameter ρ [41]. Here we plot

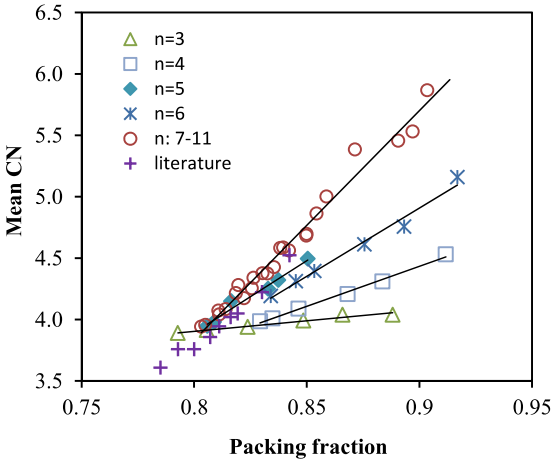

FIG. 12. (Color online) Mean coordination number as a function of packing fraction for regular polygons with different edges under different sliding friction coefficients. Literature data are from Duparcmeur *et al.* [18] for regular pentagon.

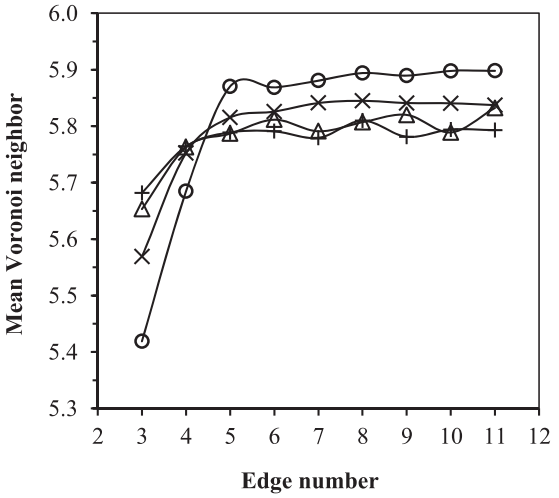

FIG. 13. The mean Voronoi neighbor per particle as a function of polygon edge number under different sliding friction coefficients: ◯, $\mu = 0.1$; ×, $\mu = 0.3$; Δ, $\mu = 0.5$; +, $\mu = 0.9$.

ρ and $\langle CN \rangle$ for the packings of regular polygons in Fig. 12. Interestingly ρ presents a simple positive linear correlation with $\langle CN \rangle$ for each kind of polygon with different μ. However, the slope of the linear correlation is dependent on n. For G1 polygons, regular triangle has the flattest slope, whereas square has a steeper slope and regular hexagon the steepest, in accordance with the effect of μ on $\langle CN \rangle$. For G2, regular pentagon has a similar slope as that of regular hexagon. Note that the results are comparable to a previous study of the random close packing of regular polygons [18]. When $n \geqslant 7$, the slopes are even steeper than those of regular hexagon but rather similar for different n. This finding indicates that the relationship between local structures and the global packing fraction could be different for different polygons, especially when $n < 7$.

D. Voronoi analysis

We use the aforementioned digitizing method to obtain the Voronoi tessellation for each particle in a packing. The accuracy of such method is dependent on the dimensions of the pixels. To test how small is enough for the pixels, we have tried different-sized pixels to digitize random orientated polygons, and the areas of the pixels inside the polygons are summed and compared to the theoretical areas of the polygons. It is found that reasonable accuracy with less than 1% can be obtained by choosing a pixel of dimensions $0.025d \times 0.025d$. After obtaining the Voronoi tessellations as shown in Fig. 5(c), we perform analysis on both their topological property (neighbor) and metrical property (area).

1. Voronoi neighbor

Two particles are regarded as Voronoi neighbors to each other if their Voronoi tessellations share a boundary. The number of Voronoi neighbors for a particle is defined as VN, which is similar to but different from CN, as it is not necessary for a Voronoi neighbor to be in contact with the given particle. Figure 13 shows that the mean Voronoi neighbor number $\langle VN \rangle$ increases with polygon edge number sharply from $n = 3$ to $n = 5$, and then almost levels off at a constant value. Such a constant value is about 5.9 when $\mu = 0.1$ but decreases with the increase of μ. At $\mu = 0.9$, $\langle VN \rangle$ is all about 5.8 when $n \geqslant 5$. This again indicates that the local structures for the packings of regular polygons of five or more edges will mainly be like a hexagonal lattice, with six particles enclosing a center one, as observed in Fig. 6. However, the real contact number, i.e., $\langle CN \rangle$ could be smaller and more sensitive to n and μ, as a polygon may needs to contact with fewer particles to be mechanically stable. That is, when $n \geqslant 5$, regular polygons could be mostly caged in a hexagonal lattice as speculated in other studies [17,32], but could have different CN depending on their shapes. The slight gap of $\langle VN \rangle$ from 6 is due to some very irregular local arrangements in the packings, which are small in ratio but will be increased by the increase of μ. On the other hand, for regular triangle and square, $\langle VN \rangle$ is significantly lower than 6 and decreases with the decrease of μ, as these two polygons will have their specific local structures which are very different from the hexagonal lattice and these local structures will be enhanced by a lower friction.

2. Voronoi area

We divide the area of a Voronoi tessellation by that of the enclosed particle, and obtain the reduced Voronoi area α. Its reciprocal can be regarded as the local packing fraction, which has been used in Fig. 6. For a packing of identical particles the global packing fraction can be given as $\rho = 1/\langle \alpha \rangle$. To find the relationship between the local and global packing fractions is important to the theoretical modeling of packings [12,13,23,42], while it is found that the Voronoi area or volume can be better modeled than local packing fraction. For generality, here we use the reduced free Voronoi area as $\zeta = \alpha - 1$, and thus make ζ start from 0. Such a concept is often used in the amorphous systems. Figure 14 demonstrates the distributions of ζ for different regular polygons. It is found that these distributions can always be described by log-normal

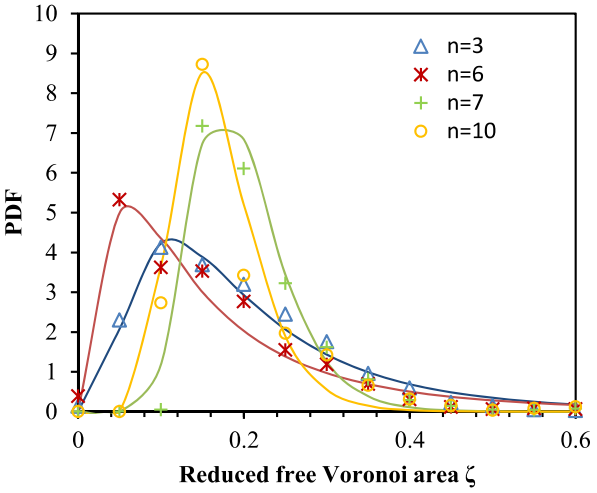

FIG. 14. (Color online) Probability distributions of the reduced free areas of Voronoi tessellations for the packings of different regular polygons ($\mu = 0.3$). Lines are the fitted log-normal distributions.

distributions given by

$$f(\zeta) = \frac{1}{\sigma\sqrt{2\pi}\zeta} \exp[-(\ln\zeta - v)^2/2\sigma^2], \qquad (1)$$

where $f(\zeta)$ is the probability density; v and σ are the geometrical parameters for the distribution, which are fitted for each packing. Such findings are in agreement with the distributions of reduced Voronoi volume for the packings of spherical particles [7]. In other studies, there are some different distributions applied, e.g., the gamma distribution of the scaled Voronoi volume in the jamming of spheres [8,12] and the Gaussian distribution of the local packing fraction for the packings of ellipsoidal particles [42]. The differences probably result from the different distribution variables used and the different packing systems considered which deserve further study. Notably here the log-normal distribution is observed by all the studied regular polygons.

The log-normal distributions are just controlled by the two parameters v and σ, while their dependencies on the edge number and the sliding friction coefficient are given in Fig. 15. It can be seen that, still, they can be clearly divided into G1 and G2. In both groups, v decreases with the increase of n and the decrease of μ, while the effect of μ is more profound for G1 polygons. On the other hand, σ is significantly larger for G1 polygons, and also changes more remarkably with the varying μ, whereas σ for G2 polygons only slightly increases with n increasing, and nearly collapses for different μ except for the lowest μ. For an ideal log-normal distribution defined by Eq. (1), the mean and variance of ζ can be given by $e^{v+\sigma^2}$ and $(e^{\sigma^2} - 1)e^{v+\sigma^2}$, respectively. We thus calculate the mean ζ and then the packing fraction according to $\rho = 1/(\langle\zeta\rangle + 1)$. The calculated packing fractions are compared to the simulated ones in Fig. 16(a). The errors are within $\pm 5\%$, which demonstrates the accuracy of the log-normal distribution fitting. It can be seen that normally ρ is underestimated, which is because the ideal log-normal distribution has an infinite long tail with $\zeta \to \infty$, whereas actually ζ has an upper bound due to the stability limit. Hence the mean ζ of the distribution will be higher than the real mean ζ, resulting in a lower ρ. The variance of ζ has also been calculated and shown in Fig. 16(b), from which it can be seen that the distributions are significantly more dispersed for G1 polygons than those of G2 polygons. This is probably because for G1 polygons the densely and loosely packed regions are more different in ζ than those for G2 polygons. Thus the variances of ζ for G1 polygons also undergo a more complicated change with μ.

E. Bond-orientational order Q_6

In parallel to the translational order, the orientational order can be evaluated by the so-called bond-orientational order based on a particle and its neighbors [6,25,32,43]. The n-fold bond-orientational order of particle j can be described by [32]

$$q_n^j = \left| \frac{1}{N_j} \sum_{k=1}^{N_j} e^{ni\theta_{jk}} \right|, \qquad (2)$$

where k is a neighbor particle of j, N_j is the number of the neighbors, and θ_{jk} is the angle between an arbitrary fixed axis

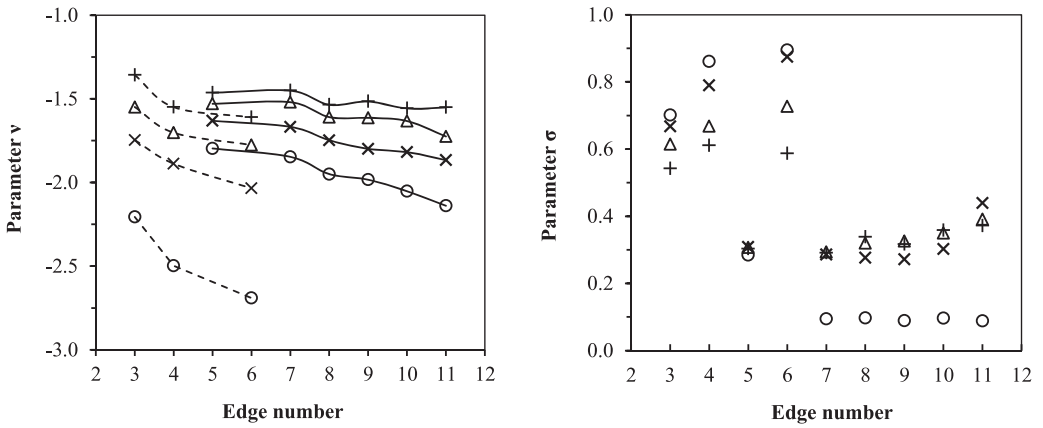

(a) (b)

FIG. 15. Parameters v and σ for the log-normal distribution as a function of polygon edge number under different sliding friction coefficients: ◯, $\mu = 0.1$; ×, $\mu = 0.3$; Δ, $\mu = 0.5$; +, $\mu = 0.9$.

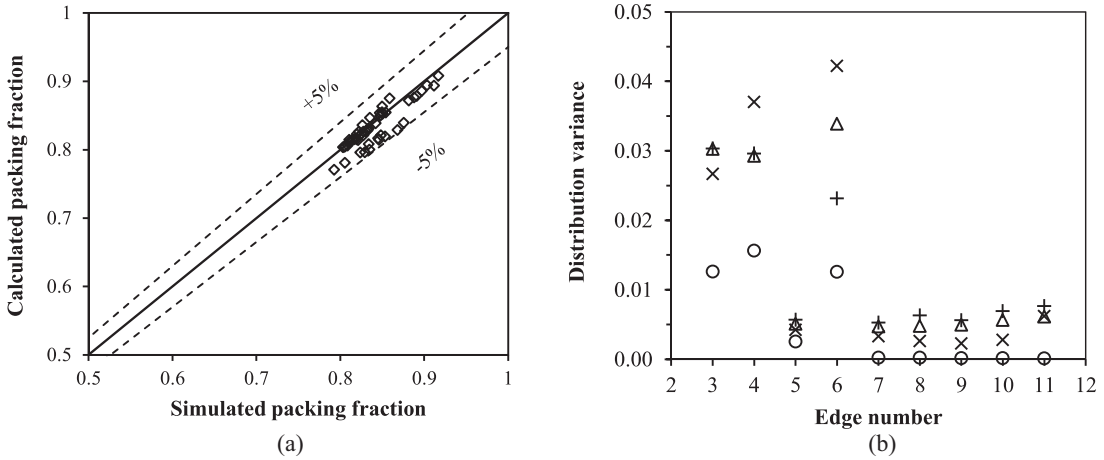

FIG. 16. (a) Calculated packing fraction (from the mean value of the log-normal distributions of free Voronoi area) versus simulated packing fraction. (b) Variances of the log-normal distributions as a function of polygon edge number under different sliding friction coefficients: ◯, $\mu = 0.1$; ×, $\mu = 0.3$; Δ, $\mu = 0.5$; +, $\mu = 0.9$.

and the vertex from particle j to k. The mean local bond-orientational order is averaged over all particles as $Q_n = q_n^j = \frac{1}{N}\sum q_n^j$, where N is the particle number. Since in the previous analyses we find the hexagonal lattice structure is most favorable in our packings, we focus on the analysis of Q_6 here.

Figure 17 shows that with a fixed sliding friction coefficient, generally Q_6, increases sharply with the edge number up to $n = 6$ and then almost levels off. The decrease of μ always increases Q_6, which is the same as its effect on the translational order. Regular triangle and square have significantly low Q_6 as they do not pack into hexagonal lattices. Regular pentagon yields a relatively higher Q_6 but still obviously lower than those with $n \geqslant 6$, suggesting that in the packing of regular pentagons, local bond-orientational orders are close to but still a certain distance from the sixfold symmetry. This can be related to the RDF peaks of regular pentagon packings in Fig. 8, in which the first peak representing the sixfold symmetric configuration is not much stronger than the second peak. On the other hand, for $n \geqslant 6$, Q_6 almost flattens out, indicating that the regular polygons with more than six edges also tend to form the hexagonal lattice structures as regular hexagon, which is consistent with other analyses. And when μ is low, Q_6 almost reaches 1.0 for $n \geqslant 6$, showing an almost perfect sixfold symmetry for the particle-neighbor bonds. However, as shown in the above analyses, particles themselves will have disordered orientations which result in distortions in the lattices and hence different packing fractions. But these disordered orientations are not considered in Q_6 since the bond-orientational order is dependent only on the bonds connecting the centers of two particles. It is thus expected that a more comprehensive orientational order parameter can be proposed for nonspherical particles.

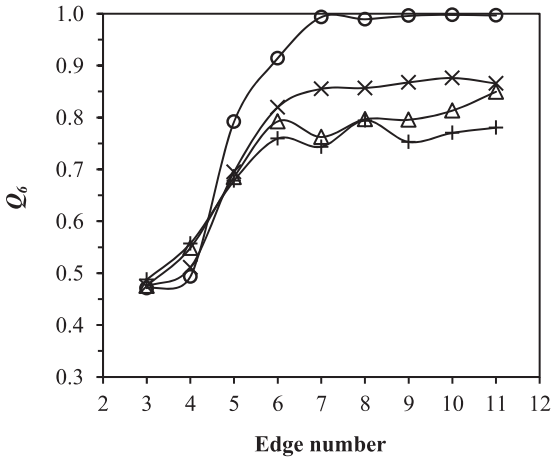

FIG. 17. The sixfold bond-orientational order Q_6 as a function of polygon edge number under different sliding friction coefficients: ◯, $\mu = 0.1$; ×, $\mu = 0.3$; Δ, $\mu = 0.5$; +, $\mu = 0.9$.

IV. CONCLUSION

We have simulated the packings of 2D granular regular polygons by using a recently developed DEM-based numerical model. The effects of shape and friction on the packing structures have been quantitatively analyzed both globally and locally. In general, the group of geometrically nonfrustrated polygons, including regular triangle, square, and hexagon, have higher packing fractions than the other group consisting of geometrically frustrated polygons. In the first group, ρ increases with the increase of edge number n, while in the second group, ρ is the lowest at $n = 7$ and approaches the maximum ρ of disks with the increase of n. The decrease of sliding friction coefficient μ always increases ρ.

The changes in ρ have been linked with the microstructure quantities in terms of radial distribution function, coordination number, Voronoi tessellation, and bond-orientational order. Specifically, the characteristic peaks in the RDF become more distinguished with the increase of n and the decrease of μ, while their positions are only dependent on n. Generally the stronger peaks represent the increase in the translational order which leads to the increase of ρ. On the other hand, Q_6 increases with the increase of n and the decrease of μ, indicating the increase of the sixfold bond-orientational order

as well. The increase of μ decreases the mean coordination number, and its effect is more profound for polygons with a higher n. Interestingly there is a positive linear relationship between $\langle CN \rangle$ and ρ while the slope is dependent on n. Free areas of Voronoi tessellations, which can be related to the local packing fractions, are found to always present a log-normal distribution form. The effects of n and μ on the distribution parameters are quantified.

These analyses establish a clearer picture for the microstructure of the packings of regular polygons and provide more comprehensive relationships between the microstructure and the global packing fraction, which can pave a way to the theoretical modeling of the effects of shape and friction on the packing structures of nonspherical particles.

Finally we should note that the simulated packings in this work are obtained with a well-defined packing method, which is comparable to pour packing under gravity. The structures of some of these packings have been shown to be comparable to those obtained using other methods in terms of packing fraction and some structural parameters, whereas we cannot assert that these packings are method independent. In the last two decades, it is found that for the packings of uniform spheres, there are several critical packing states with reproducible packing fractions, which are independent of packing protocols but represent the critical structure changes of the system. For example, random close packing (RCP) originally defined from the packing method can be more precisely defined as the maximally random jammed (MRJ) state by using certain structural parameters [43]. But currently it is not clear if these states also exist in other packing systems such as the packings of polygons. We think the critical packing states for nonspherical particles will be much more complicated than those for uniform spheres, which are actually not the focus of this work. However, we believe that the improved understandings of the structures of the nonsphere packings, as presented in this work, could help achieve such findings in the future.

ACKNOWLEDGMENT

The authors are grateful to Australian Research Council (Grant No. DE120100960) for the financial support of this work.

[1] H. M. Jaeger, S. R. Nagel, and R. P. Behringer, Rev. Mod. Phys. **68**, 1259 (1996).
[2] R. M. German, *Particle Packing Characteristics* (Metal Powder Industries Federations, Princeton, New Jersey, 1989).
[3] S. Torquato and F. H. Stillinger, Rev. Mod. Phys. **82**, 2633 (2010).
[4] A. J. Liu and S. R. Nagel, Nature **396**, 21 (1998).
[5] L. Y. Yi, K. J. Dong, R. P. Zou, and A. B. Yu, Powder Technol. **224**, 129 (2012).
[6] K. J. Dong, R. Y. Yang, R. P. Zou, and A. B. Yu, Phys. Rev. Lett. **96**, 145505 (2006).
[7] R. Y. Yang, R. P. Zou, and A. B. Yu, Phys. Rev. E **65**, 041302 (2002).
[8] T. Aste and T. Di Matteo, Phys. Rev. E **77**, 021309 (2008).
[9] Z. A. Tian, K. J. Dong, and A. B. Yu, Phys. Rev. E **89**, 032202 (2014).
[10] A. V. Anikeenko and N. N. Medvedev, Phys. Rev. Lett. **98**, 235504 (2007).
[11] K. J. Dong, R. Y. Yang, R. P. Zou, X. Z. An, and A. B. Yu, EPL **86**, 6 (2009).
[12] A. V. Anikeenko, N. N. Medvedev, and T. Aste, Phys. Rev. E **77**, 031101 (2008).
[13] C. Song, P. Wang, and H. A. Makse, Nature **453**, 629 (2008).
[14] A. Donev, I. Cisse, D. Sachs, E. A. Variano, F. H. Stillinger, R. Connelly, S. Torquato, and P. M. Chaikin, Science **303**, 990 (2004).
[15] R. Guises, J. Xiang, J.-P. Latham, and A. Munjiza, Granul. Matter **11**, 281 (2009).
[16] K. Stokely, A. Diacou, and S. V. Franklin, Phys. Rev. E **67**, 051302 (2003).
[17] Y. L. Duparcmeur, A. Gervois, and J. Troadec, J. de Physique I **5**, 1539 (1995).
[18] Y. L. Duparcmeur, J. P. Troadec, and A. Gervois, J. de Physique I **7**, 1181 (1997).
[19] A. A. Mirghasemi, L. Rothenburg, and E. L. Matyas, Geotechnique **52**, 209 (2002).
[20] S. Torquato and Y. Jiao, Nature **460**, 876 (2009).
[21] A. Jaoshvili, A. Esakia, M. Porrati, and P. M. Chaikin, Phys. Rev. Lett. **104**, 185501 (2010).
[22] Z. Y. Zhou, R. P. Zou, D. Pinson, and A. B. Yu, Ind. Eng. Chem. Res. **50**, 9787 (2011).
[23] A. Baule, R. Mari, L. Bo, L. Portal, and H. A. Makse, Nat. Commun. **4**, 2194 (2013).
[24] R. P. Zou and A. B. Yu, Powder Technol. **88**, 71 (1996).
[25] K. Zhao and T. G. Mason, Phys. Rev. Lett. **103**, 208302 (2009).
[26] K. Zhao, R. Bruinsma, and T. G. Mason, Nat. Commun. **3**, 801 (2012).
[27] C. L. Henley, Phys. Rev. B **34**, 797 (1986).
[28] M. Cieśla and J. Barbasz, Phys. Rev. E **90**, 022402 (2014).
[29] D.-H. Nguyen, E. Azéma, F. Radjai, and P. Sornay, Phys. Rev. E **90**, 012202 (2014).
[30] V. A. Luchnikov, N. N. Medvedev, L. Oger, and J. P. Troadec, Phys. Rev. E **59**, 7205 (1999).
[31] F. M. Schaller, S. C. Kapfer, M. E. Evans, M. J. Hoffmann, T. Aste, M. Saadatfar, K. Mecke, G. W. Delaney, and G. E. Schröder-Turk, Philos. Mag. **93**, 3993 (2013).
[32] T. Schilling, S. Pronk, B. Mulder, and D. Frenkel, Phys. Rev. E **71**, 036138 (2005).
[33] M. Mailman, C. F. Schreck, C. S. O'Hern, and B. Chakraborty, Phys. Rev. Lett. **102**, 255501 (2009).
[34] X. Z. An, R. Y. Yang, K. J. Dong, R. P. Zou, and A. B. Yu, Phys. Rev. Lett. **95**, 205502 (2005).
[35] L. Y. Yi, K. J. Dong, R. P. Zou, and A. B. Yu, Ind. Eng. Chem. Res. **50**, 8773 (2011).
[36] K. J. Dong, C. C. Wang, and A. B. Yu, Chem. Eng. Sci. **126**, 500 (2015).
[37] C. H. Rycroft, Chaos **19**, 041111 (2009).

[38] N. N. Medvedev, V. P. Voloshin, V. A. Luchnikov, and M. L. Gavrilova, J. Comput. Chem. **27**, 1676 (2006).

[39] R. Al-Raoush and K. A. Alshibli, Phys. A: Statistical Mechanics and its Applications **361**, 441 (2006).

[40] C. M. Carlevaro and L. A. Pugnaloni, J. Stat. Mech.: Theory and Experiment (2011) P01007.

[41] L. W. Rong, K. J. Dong, and A. B. Yu, Chem. Eng. Sci. **99**, 44 (2013).

[42] F. M. Schaller, M. Neudecker, M. Saadatfar, G. W. Delaney, G. E. Schröder-Turk, and M. Schröter, Phys. Rev. Lett. **114**, 158001 (2015).

[43] S. Torquato, T. M. Truskett, and P. G. Debenedetti, Phys. Rev. Lett. **84**, 2064 (2000).